



CHORUS

This is the accepted manuscript made available via CHORUS. The article has been published as:

Sub-Ohmic to super-Ohmic crossover behavior in nonequilibrium quantum systems with electron-phonon interactions

Eli Y. Wilner, Haobin Wang, Michael Thoss, and Eran Rabani

Phys. Rev. B **92**, 195143 — Published 20 November 2015

DOI: [10.1103/PhysRevB.92.195143](https://doi.org/10.1103/PhysRevB.92.195143)

Sub-Ohmic to super-Ohmic crossover behavior in nonequilibrium quantum systems with electron-phonon interactions

Eli Y. Wilner,¹ Haobin Wang,² Michael Thoss,³ and Eran Rabani^{4,5}

¹*School of Physics and Astronomy, The Sackler Faculty of Exact Sciences, Tel Aviv University, Tel Aviv 69978, Israel*

²*Department of Chemistry, University of Colorado Denver, Denver, Colorado 80217-3364, USA*

³*Institute for Theoretical Physics and Interdisciplinary Center for Molecular Materials, Friedrich-Alexander-Universität Erlangen-Nürnberg, Staudtstr. 7/B2, 91058 Erlangen, Germany*

⁴*Department of Chemistry, University of California and Lawrence Berkeley National Laboratory, Berkeley, California 94720, USA*

⁵*The Sackler Center for Computational Molecular and Materials Science, Tel Aviv University, Tel Aviv, Israel 69978*

The transition from weakly damped coherent motion to localization in the context of the spin-boson model has been the subject of numerous studies with distinct behavior depending on the form of the phonon-bath spectral density, $J(\omega) \propto \omega^s$. Sub-Ohmic ($s < 1$) and Ohmic ($s = 1$) spectral densities show a clear localization transition at zero temperature and zero bias, while for super-Ohmic ($s > 1$) spectral densities this transition disappears. In this work, we consider the influence of the phonon-bath spectral density on the *nonequilibrium* dynamics of a quantum dot with electron-phonon interactions described by the extended Holstein model. Using the reduced density matrix formalism combined with the multi-layer multiconfiguration time-dependent Hartree approach, we investigate the dynamic response, the time scales for relaxation, as well as the existence of multiple long-lived solutions as the system-bath coupling changes from the sub- to the super-Ohmic cases. Bistability is shown to diminish for increasing powers of s similar to the spin-boson case. However, the physical mechanism and the dependence on the model parameters such as the typical bath frequency ω_c and the polaron shift λ are rather distinct.

Introduction

Quantum dissipation is an omnipresent phenomenon in diverse physical systems, ranging from quantum information¹ and quantum optics,² to charge transfer and impurity relaxation,^{3,4} superconducting junctions,⁵ and more, spanning diverse energy, length and time scales. Describing the effects of the environment on the dynamic response of a sub-system requires both the development of theoretical and computational tools as well as the development of simplified models necessary to account for the rich system-bath dynamics and thermodynamic phase behavior. The minimal model required to capture the essential physics of quantum dissipation involves a two-level system coupled to a bosonic bath. Perhaps the most studied version is the well-known spin-boson model,⁶ where it is assumed that the two-level system is linearly coupled to a harmonic bath. The effects of the environment are characterized by the properties of the bath spectral density, assumed to have a power-law dependence at low frequencies, ω^s ($s \in \mathbb{R}^+$), with a cutoff at higher frequencies determined by a characteristic frequency, ω_c . The value of “ s ” classifies the nature of the dissipative environment, often referred to as sub-Ohmic for $0 < s < 1$, Ohmic for $s = 1$ and super-Ohmic for $s > 1$.

The dynamics, equilibrium and phase behavior of the two-level system is governed, amongst other factors, by the value of “ s ”. A notable transition from coherent to incoherent dynamics in the spin-boson model is observed as the Kondo parameter, η (dimensionless strength of the system-bath coupling) is increased or when the bath spectral density changes from super-Ohmic to sub-Ohmic.^{4,7,8}

This is followed by a localization transition at high values of η in the limit $\omega_c \rightarrow \infty$ and low temperature, $T \rightarrow 0$, for the sub-Ohmic and Ohmic cases. Such a transition disappears for^{4,6,9–12} $s > 1$. This rich behavior has been investigated by a variety of theoretical approaches including analytical^{13–16} and approximate numerical techniques (for an overview, see Refs. 4,6) as well as numerically exact methods such as numerical renormalization group (NRG) techniques,^{11,17–19} the multi-configuration time-dependent Hartree (MCTDH) approach and its multilayer (ML) extension, ML-MCTDH,^{20–22} and path-integral methods.^{4,23–26}

The dynamics and steady-state properties of dissipative quantum systems driven away from equilibrium have been the center of more recent studies, e.g. for driven spin-boson-type systems,²⁷ or in the context of inelastic tunneling in quantum point contacts and molecular junctions.^{28–37} The canonical model in the latter field is given by the extended Holstein model,³⁸ in which a bridge level (occupied or empty, hence two levels) is coupled to a bosonic bath, describing the phonons, and in addition to two fermionic reservoirs representing the left and right leads. The latter are held at a different chemical potentials and thus provide the source to drive the system away from equilibrium. Most studies focused on steady-state properties utilizing a variety of techniques to describe, e.g., Franck-Condon blockade,^{39–43} negative differential resistance,^{44–48} or the existence of multiple long-lived solutions, i.e. bistability.^{49–57} In addition, novel numerically exact techniques uncovered interesting transient behavior.^{56,58–61} A promising approach in this regard is the combination of the reduced density matrix approach^{62,63} and the multilayer multiconfiguration

time-dependent Hartree method in second quantized representation (ML-MCTDH-SQR),⁵⁹ used to explore the timescales and the dynamic “phase diagram” associated with the bistability.^{57,59,64,65} The most striking result reported by Wilner *et al.*⁶⁴ for the extended Holstein model with an Ohmic spectral density is that the bistability persists on timescales exceeding the phonon-assisted tunneling time along the adiabatic potential.

At first glance, the localization transition in the spin-boson model and the bistability in the nonequilibrium extended Holstein model may result from similar physics. However, these phenomena are quite different in nature and origin. First, localization in the spin-boson model is a quantum phase transition strictly at $T = 0$, while bistability is a transient phenomenon persisting over a range of source-drain bias voltages. Second, the former vanishes in the adiabatic limit of a slow bath ($\omega_c \rightarrow 0$) while the latter thrives in this limit. Finally, in the Ohmic case, localization due to a degenerate ground state and the corresponding dependence of the steady state on the initial state occurs only for the symmetric spin-boson model, while bistability in the extended Holstein model spans a wide range of asymmetries

In this work, we explore the dependence of bistability on the nature of the phonon spectral density using the combined ML-MCTDH-SQR and reduced density matrix approach. We cover both the the sub-Ohmic to super-Ohmic limits. While localization and bistability show opposite behavior with respect to ω_c , we find similarities with respect to the boson spectral density. Specifically, as s is increased above 1 the bistability diminishes. This transition, however, is not as sharp as the localization transition.

Model Hamiltonian and Spectral Densities

To describe the effect of different forms of dissipation on nonequilibrium transport in a quantum system with electron-phonon interaction, we consider a generic model Hamiltonian describing, e.g., a quantum dot or a molecular junction:

$$H = H_S + H_B + V_{SB}. \quad (1)$$

Here, $H_S = \varepsilon_d d^\dagger d$ is the system Hamiltonian representing the electronic degrees of freedom of the quantum dot with creation/annihilation fermionic operators d^\dagger/d and energy ε_d . For simplicity, we assume that the quantum dot is represented by a single level. The bath Hamiltonian, $H_B = H_\ell + H_{ph}$, is given as a sum of electron (lead) and phonon baths where

$$H_\ell = \sum_{k \in L,R} \varepsilon_k a_k^\dagger a_k \quad (2)$$

represents the noninteracting leads Hamiltonian with fermionic creation/annihilation operators a_k^\dagger/a_k , and

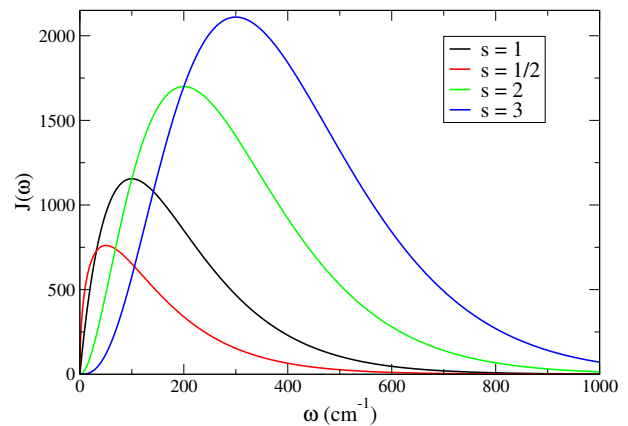


Figure 1: The phonon spectral density, $J(\omega) = \frac{\lambda\pi\omega^s}{\Gamma(s)\omega_c^s} e^{-\frac{\omega}{\omega_c}}$, for various values of s for $\omega_c = 100\text{cm}^{-1}$ and $\lambda = 1000\text{cm}^{-1}$.

$$H_{ph} = \sum_j \hbar\omega_j \left(b_j^\dagger b_j + \frac{1}{2} \right) \quad (3)$$

represents the phonon bath with creation/annihilation bosonic operators b_j^\dagger/b_j for phonon mode α with energy $\hbar\omega_j$. The coupling between the system and the baths is given by

$$V_{SB} = \sum_{k \in L,R} \left(t_k d a_k^\dagger + t_k^* a_k d^\dagger \right) + d^\dagger d \sum_j M_j \left(b_j^\dagger + b_j \right) \quad (4)$$

where t_k is the hopping term between the system and the leads and M_α is the strength of the electron-phonon couplings to mode α . The former is determined from the relation

$$\Gamma_{L,R}(\varepsilon) = 2\pi \sum_{k \in L,R} |t_k|^2 \delta(\varepsilon - \varepsilon_k), \quad (5)$$

with $\Gamma_{L,R}(\varepsilon) = \frac{a^2}{b^2} \sqrt{4b^2 - (\varepsilon - \mu_{L,R})^2}$ used to mimic a tight-binding chain and $\mu_{L,R}$ is the chemical potential of the left/right lead, respectively. We adopt the same parameters for $\Gamma_{L,R}(\varepsilon)$ used in our recent studies,^{57,64} namely, $a = 0.2\text{eV}$ and $b = 1\text{eV}$. For this choice, $\Gamma = 0.16\text{eV}$ is the maximum value of $\Gamma_R(\varepsilon) + \Gamma_L(\varepsilon)$. The electron-phonon couplings, M_α , are determined from the relation:

$$J(\omega) = \pi \sum_j M_j^2 \delta(\hbar\omega - \hbar\omega_j) \quad (6)$$

where we follow the notation of Caldeira and Leggett⁶⁶ for the phonon spectral density:

$$J(\omega) = \frac{\pi\hbar}{2} \eta \left(\omega^s / \omega_c^{s-1} \right) e^{-\frac{\omega}{\omega_c}}. \quad (7)$$

In the above equation, the dimensionless Kondo parameter, $\eta = \frac{2\lambda}{\hbar\omega_c\Gamma(s)}$, determines the overall strength of

the electron-phonon couplings, ω_c is the characteristic phonon bath frequency and $\Gamma(s)$ is the Euler Gamma function. For future reference, we introduce an additional parameter $\lambda = \sum_j \frac{M_j^2}{\hbar\omega_j} = \frac{1}{\pi} \int \frac{d\omega}{\omega} J(\omega)$, which is known as the reorganization energy (or polaron shift). Fig. 1 shows the results for $J(\omega)$ for different values of s .

The model introduced above and variants thereof have been widely used to study nonequilibrium charge transport in nanostructures, such as, for example, semiconductor quantum dots,⁶⁷ carbon nanotubes⁶⁸ or molecular junctions.^{50,69–73} In the latter case, the phonons may include, in addition to the phonons of the contacts, the vibrational degrees of freedom of the molecule. In all previous studies, however, the spectral density was limited to the Ohmic case, for which $s = 1$. The sub-Ohmic ($s < 1$) and super-Ohmic ($s > 1$) limits which play an important role in the related spin-boson model,⁴ have not been studied in transport junctions.

Reduced Density Matrix

The dynamics generated by the above Hamiltonian are rich and rather complicated to solve. Numerically exact techniques include real time path integrations^{43,58,61,74–79} and ML-MCTDH approach.^{20–22} Both are limited to relatively short times and cannot describe the dynamics on all relevant timescales. Recently, we have proposed to combine a numerically exact impurity solver with a reduced density matrix formalism.^{57,62–64,80} Application to the above model for the Ohmic spectral density uncovered a fascinating behavior with rich dynamics on multiple timescales and bistability persisting on timescale longer than the phonon-assisted tunneling times.^{57,64,65} Here, we adopt this approach to study the influence of different forms of the phonon spectral density on the dynamic response and on the bistability. For completeness, we briefly review the formalism.

The basic quantity of interest is the reduced density matrix, $\sigma(t)$, which is derived from the full density matrix, $\rho(t)$, by the application of the projection operator $P = \rho_B Tr_B$. Here, the index B refers to the bath degrees of freedom or the “irrelevant” part of the full Hamiltonian. $\sigma(t) = Tr_B \rho(t)$ obeys a generalized quantum master equation, given by:⁸¹

$$i\hbar \frac{\partial}{\partial t} \sigma(t) = \mathcal{L}_S \sigma(t) + \vartheta(t) - \frac{i}{\hbar} \int_0^t d\tau \kappa(\tau) \sigma(t - \tau). \quad (8)$$

where $\mathcal{L}_S = [H_S, \dots]$ is the system’s Liouvillian,

$$\vartheta(t) = Tr_B \left\{ \mathcal{L}_V e^{-\frac{i}{\hbar} Q \mathcal{L} t} Q \rho(0) \right\} \quad (9)$$

depends on the choice of initial conditions and vanishes for an uncorrelated initial state (which is the case considered below), *i.e.*, when $\rho(0) = \sigma(0) \otimes \rho_B(0)$, where $\sigma(0)$ and $\rho_B(0)$ are the system and bath initial density matrices, respectively, and $\mathcal{L}_v = [V_{SB}, \dots]$. We consider two

initial conditions for $\sigma(0)$, an occupied and unoccupied dot. We assume a non-correlated initial state for $\rho_B(0)$

$$\rho_B(0) = \rho_{\text{ph}}(0) \otimes \rho_\ell^L(0) \otimes \rho_\ell^R(0), \quad (10)$$

where ($\beta = \frac{1}{k_B T}$ is the inverse temperature)

$$\rho_\ell^{L/R}(0) = \exp \left[-\beta \left(\sum_{k \in L/R} (\varepsilon_k - \mu_{L/R}) a_k^\dagger a_k \right) \right], \quad (11)$$

is the initial density matrix for the leads, and

$$\rho_{\text{ph}}(0) = \exp \left[-\beta \left\{ \sum_\alpha \hbar\omega_j \left(b_j^\dagger b_j + \frac{1}{2} \right) + \sum_j \delta_j M_j \left(b_j^\dagger + b_j \right) \right\} \right] \quad (12)$$

represents the initial density matrix of the phonon bath. We also consider two different initial conditions for the phonons, one where $\delta_j = 0$ in Eq. (12) corresponding to phonons initially equilibrated with an unoccupied dot, and another where $\delta_j = 1$ corresponding to phonons equilibrated to an occupied dot. More details can be found in Ref. 57.

The calculations of the memory kernel in Eq. (8), $\kappa(t)$, is the tricky part. Formally it is given by

$$\kappa(t) = Tr_B \left\{ \mathcal{L}_V e^{-\frac{i}{\hbar} Q \mathcal{L} t} Q \mathcal{L} \rho_B \right\} \quad (13)$$

where $Q = 1 - P$, $P = \rho_B(0) Tr_B \{ \dots \}$ and $\mathcal{L} = [H, \dots]$. A more suitable form for the memory is given in terms of a Volterra equation of the second type, removing the complexity of the projected dynamics of Eq. (13):

$$\kappa(t) = i\hbar \dot{\Phi}(t) - \Phi(t) \mathcal{L}_S + \frac{i}{\hbar} \int_0^t d\tau \Phi(t - \tau) \kappa(\tau) \quad (14)$$

with $\Phi(t) = Tr_B (\mathcal{L}_V e^{-\frac{i}{\hbar} \mathcal{L} t} \rho_B)$. For the present model, the coherence do not couple to the populations.⁵⁷ Thus, only the $\Phi_{nn,mm}$ elements are required to obtain the populations. It can be shown⁵⁷ that only the dot-lead interactions in \mathcal{L}_V contributes to these elements:

$$\Phi_{nn,mm}(t) = \frac{2}{\hbar} Tr_B \left\{ \rho_B \langle m | \sum_k t_k d(t) a_k^\dagger(t) | m \rangle \right\} .. \quad (15)$$

Here, $|m\rangle$ denotes the electronic state of the quantum dot, where m can take the values 1 or 0, corresponding to an occupied or an unoccupied dot, respectively. Previously, we have shown that $\Phi_{nn,mm}(t)$ can be expressed in terms of the sum of the left ($I_m^L(t)$) and right ($I_m^R(t)$) currents:

$$e\Phi_{nn,mm}(t) = I_m^L(t) + I_m^R(t), \quad (16)$$

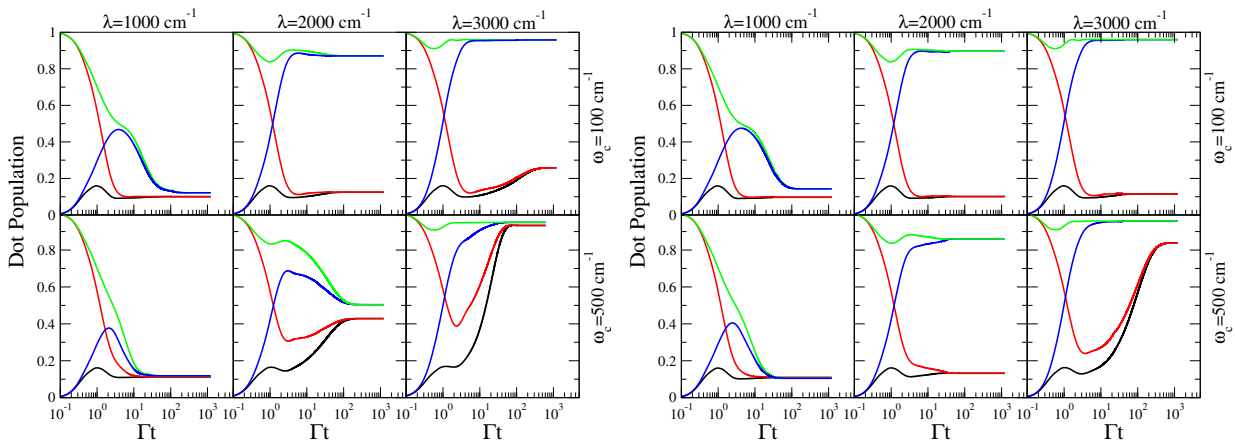


Figure 2: Transient dynamics of the average quantum dot population for the Ohmic (left set of panels, $s = 1$) and sub-Ohmic case (right set of panels, $s = 1/2$). The results are shown for all 4 initial conditions: Black and red curves correspond to unoccupied / occupied dot at phonon initial condition $\delta_j = 0$, whereas blue and green curves correspond to unoccupied / occupied at $\delta_j = 1$, respectively. In all results the cutoff time used to generate the memory kernel is $t_c = 100$ fs.

where

$$I_m^{L,R}(t) = -\frac{2e}{\hbar} \Im \sum_{k \in L,R} t_k \langle m | d(t) a_k^\dagger(t) | m \rangle, \quad (17)$$

is the left/right current for an initial occupied ($m = 1$) or empty ($m = 0$) dot, and e is the electron charge.

While the calculation of the memory kernel requires a solution of the time-dependent left and right currents, it typically decays on timescales much faster than the density matrix itself,^{57,62} and thus is amenable to a numerically exact impurity solvers. For this purpose we adopt the ML-MCTDH approach^{20–22} and calculate the memory up to a cutoff time t_c , where t_c is large enough such that the results for the reduced density matrix do not change for large cutoff times. When suitable, i.e., for small electron-phonon couplings,⁶⁴ we often use the nonequilibrium Green’s function formalism within the self-consistent Born approximation to generate the memory kernel for $t < t_c$.

Sub-Ohmic and Ohmic cases

In Fig. 2 we show the populations dynamics for the Ohmic ($s = 1$) and sub-Ohmic ($s = \frac{1}{2}$) cases for various values of the reorganization parameter λ and the phonon frequency ω_c . Throughout this work we fix the electronic parameters: Dot energy $\varepsilon_d = 0.25$ eV, applied bias-voltage $\mu_L = -\mu_R = 0.05$ eV and zero temperature ($k_B T = 0$). These parameters were chosen to ensure the existence of a bistability for the Ohmic case.⁶⁴ The results shown for the Ohmic case (left set of panels in Fig. 2) summarize our previous findings.^{57,64} In short, the decay of the population is characterized by three distinct timescales. At short to intermediate times, the population dynamics are governed by the system-lead hybridization \hbar/Γ (as clearly seen for $\delta_j = 0$, $\lambda = 1000$ cm⁻¹)

or by ω_c^{-1} (as clearly seen for $\delta_j = 1$, $\lambda = 1000$ cm⁻¹). In addition to the short and intermediate timescales associated with the separate electronic and phononic degrees of freedom, the electron-phonon coupling introduces longer timescales related to the tunneling between the two charge states, as clearly evident for increasing values of λ . On timescale longer than this tunneling time, the population is characterized by two distinct, long-lived, solutions for large values of λ . This “bistability” vanishes as the system become less adiabatic (increasing ω_c) or for small polaron shifts (small λ). Readers interested in a comprehensive discussion of the Ohmic case are encouraged to consult Ref. 64.

The situation is similar for the sub-Ohmic case (right set of panels in Fig. 2). All three timescales are clearly observed even for $s = \frac{1}{2}$. For $\lambda = 1000$ cm⁻¹ $< \varepsilon_d$, the more stable solution is associated with the non-shifted configuration ($\delta_j = 0$) and the system relaxes to a single long-lived state regardless of the choice of initial condition ($\delta_j = 0$ or 1). The dynamics at short and intermediate times are governed by \hbar/Γ for the non-shifted phonon bath ($\delta_j = 0$), since the dot energy $\varepsilon_d = 0.25$ eV is outside the conduction window ($\Delta\mu = 0.1$ eV) and thus the system remains in the uncharged state. This is not the case for the shifted bath initial preparation ($\delta_j = 1$). Since the effective dot energy ($\tilde{\varepsilon}_d = \varepsilon_d - 2\lambda$, Ref. 64) is within the conduction window, we observe a rapid uncharging decay associated with \hbar/Γ followed by a slower relaxation to the stable uncharged configuration along the generalized bath mode, characterized by $1/\omega_c$ timescale.

As λ increases above ε_d , the long-time behavior of the population depends on the choice of the initial phonon preparation, leading to a bistability (two distinct long lived solutions). The bistability is rather sensitive to the characteristic phonon frequency, and can lead to two steady states solutions in the adiabatic limit, as $\omega_c \rightarrow 0$.⁵⁴ As ω_c increases the bistability gradually dis-

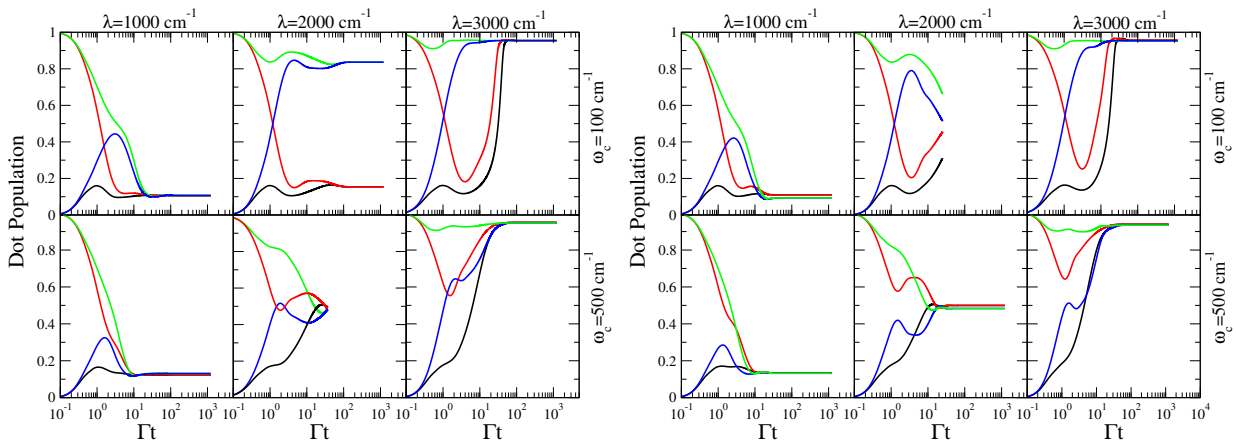


Figure 3: Transient dynamics of the average quantum dot population for the super-Ohmic case ($s = 2$ and $s = 3$ for the left and right set of panels, respectively). The results are shown for all 4 initial conditions: Black and red curves correspond to unoccupied / occupied dot at phonon initial condition $\delta_j = 0$, whereas blue and green curves correspond to unoccupied / occupied at $\delta_j = 1$, respectively. In all results the cutoff time used to generated the memory kernel is $t_c = 100$ fs. Converging the results $\omega_c = 500\text{cm}^{-1}$, $\lambda = 2000\text{cm}^{-1}$ for $s = 2$ and $\omega_c = 100\text{cm}^{-1}$, $\lambda = 2000\text{cm}^{-1}$ for $s = 3$ is difficult, and thus we only show the direct ML-MCTDH-SQR to $t = t_c$.

appears. Comparing the sub-Ohmic case to the Ohmic case, the bistability persists over a wider range of frequencies and polaron shifts for $s < 1$. This can be explained qualitatively by looking at the spectral density function shown in Fig. 1. In the sub-Ohmic case, the bath spectrum is shifted to the lower frequency end as compared with the Ohmic case that has the same characteristic frequency ω_c . Thus, a comparison of the dynamics generated for the Ohmic case at a particular values of ω_c should be done with the dynamics generated for the sub-Ohmic case ($s = 1/2$) for a higher ω_c .

To summarize the sub-Ohmic case, we find that the behavior is similar to the Ohmic case. The major difference is observed for the long time relaxation. The sub-Ohmic case shows a pronounced bistability at larger values of ω_c and a wider range of polaron shifts compared to the Ohmic case, resulting from the increase in the density of low frequency modes as s is decreased below 1.

Super-Ohmic case

The trends observed going from the sub-Ohmic case to the Ohmic case continue smoothly as s is increased above 1. In Fig. 3 we plots the transient population dynamics for the super-Ohmic case ($s = 2$ and $s = 3$) for the same set of frequencies and polaron shifts shown in Fig. 2. In two cases, we are unable to converge the results based on the memory formalism with the given input and thus, show the direct calculations based on the ML-MCTDH-SQR approach generated for $t < t_c = 100$ fs. Similar to sub-Ohmic case, for $\lambda = 1000\text{cm}^{-1}$ the population dynamics at short and intermediate times is governed by \hbar/Γ for the non-shifted phonon bath ($\delta_j = 0$) and by the typical phonon frequency for the shifted bath initial

preparation ($\delta_j = 1$). The major effect associated with changing s is the change in the characteristic phonon frequency, given by $s\omega_c$. As s increases above 1, the characteristic frequency increases leading to a rapid decay of the population at intermediate times, evident in Figs. 2 and 3. Concerning the long time behavior, we find that the tunneling dynamics are washed out as s increases above 1 and the bistability is limited to a narrower range of polaron shifts, which eventually disappears for $s \geq 3$ for the range of frequencies studied.

Comparing the behavior of the bistability to the localization transition in the spin-boson model, it is clear that the origin of the two phenomena is quite different. While in the spin-boson model localization is a quantum phase transition, observed strictly at zero temperature and zero bias, bistability is a dynamical phenomenon observed in the time-domain. Furthermore, while localization vanishes for $s > 1$, the bistability transitions smoothly across the Ohmic case. Moreover, the two phenomena differ and show opposing behavior with respect to the dependence on ω_c and to a large extent with respect to the polaron shift λ . For the latter, the bistability is limited to a certain window of λ , a window which smoothly narrows down as s increases. Localization in the spin-boson model persists above a certain value of λ .

A notable feature of the super-Ohmic case is the pronounced oscillations in the population compared to the over-damped Ohmic and sub-Ohmic behavior, as shown in the left panels of Fig. 4. This is similar to the coherent dynamics observed for the super-Ohmic case in the spin-boson model. The period of oscillations increases as the characteristic frequency of the boson bath decreases, which makes the convergence of the memory formalism difficult for ω_c values between 100 and 500 cm^{-1} due to the relatively long transient dynamics. As ω_c in-

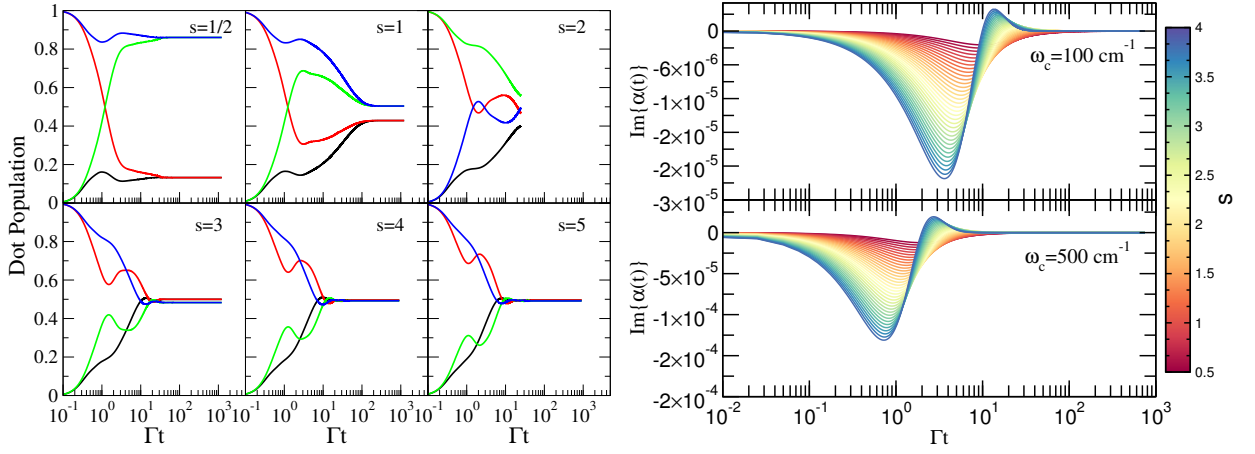


Figure 4: Left: Dot population in the super-Ohmic case for $\varepsilon_d = 0.25\text{eV}$, $\lambda = 2000\text{cm}^{-1}$ and $\omega_c = 500\text{cm}^{-1}$. The results are shown for all 4 initial conditions: Black and red curves correspond to unoccupied / occupied dot at phonon initial condition $\delta_j = 0$, whereas blue and green curves correspond to unoccupied / occupied at $\delta_j = 1$, respectively. Right: $\Im\{\alpha(t)\}$ for different value of s for $\omega_c = 100\text{cm}^{-1}$ (upper panel) and $\omega_c = 500\text{cm}^{-1}$ (lower panel).

creases, the coherence is eventually quenched because of the more efficient energy exchange between the electron and phonon degrees of freedom, as shown in Fig. 5.

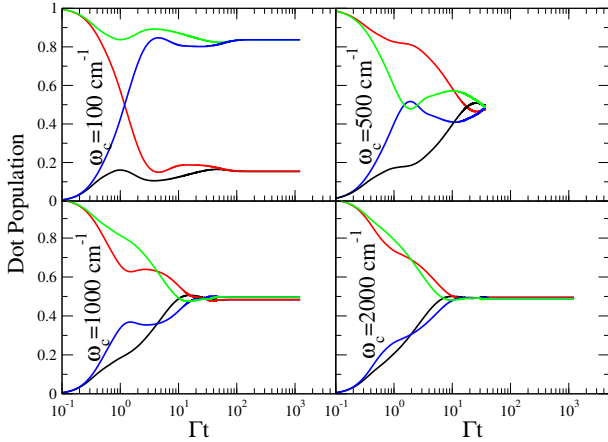


Figure 5: Coherent to incoherent transition in the super-Ohmic case $s = 2$. Shown are results of the dot population for different characteristic frequencies ω_c of the phonon bath as indicated in the plot and for four different initial condition as indicated by the different colors. The color code is the same as in Fig. 4.

To understand this behavior, we propose to examine the phonon bath autocorrelation function, given by (at $T = 0$):

$$\alpha(t) = \frac{1}{\hbar\pi} \int_0^\infty d\omega J(\omega) \exp(-i\omega t). \quad (18)$$

Using the spectral density of Eq. (6), we obtain an exact

solution to $\alpha(t)$ of the form:

$$\alpha(t) = \frac{\eta\omega_c^2}{2} \frac{\Gamma(1+s)}{(1+t^2\omega_c^2)^{\frac{s+1}{2}}} \times \exp[-i(1+s)\arctan(\omega_c t)]. \quad (19)$$

In the right panels in Fig. 4 we plot the imaginary part of $\alpha(t)$ for two values of the frequency and for different values of s . $\alpha(t)$ shows a transition from a smooth function of time at small values of $s < 1$ to an oscillatory function at larger values of $s > 1$. The origin of this oscillatory behavior is in the term $\exp[i(1+s)\arctan(\omega_c t)]$ and is correlated with the under-damped dynamics of the population shown in the left panels of Fig. 4.

A more quantitative picture of the oscillatory behavior emerges by considering the dynamics of the reaction mode $\langle Q(t) \rangle = \frac{\sum_\alpha M_\alpha \langle b_j^\dagger(t) + b_j(t) \rangle}{\sqrt{\sum_\alpha 2M_\alpha^2}}$.⁶⁵ Despite the fact that the dynamics of the phonons have been traced out by considering the reduced density matrix of the system alone, $\langle Q(t) \rangle$ for the non-shifted case ($\delta_j = 0$) can be inferred using its equation of motion, resulting in⁶⁵

$$\langle Q(t) \rangle = Q_1(t) + Q_2(t) \quad (20)$$

with

$$Q_1(t) = n_\infty \sqrt{\frac{2}{\alpha(0)}} \Im \int_0^t \alpha(\tau) d\tau \quad (21)$$

$$Q_2(t) = \sqrt{\frac{2}{\alpha(0)}} \Im \int_0^t \delta n(\tau) \alpha(t-\tau) d\tau, \quad (22)$$

where n_∞ is the steady state dot population and $\delta n(t) = \langle d^\dagger(t) d(t) \rangle - n_\infty$. A similar expression not given here can be derived for the shifted case ($\delta_j = 1$) (see appendix). The first term, Q_1 , on the right hand side of

Eq. (20) describes the relaxation of the reaction mode due to the coupling to the phonon bath in the absence of coupling to the leads. It can be calculated explicitly using Eq. (19), resulting in

$$Q_1(t) = n_\infty \sqrt{\frac{2\lambda}{s\hbar\omega_c}} \left(\frac{\cos(s \arctan(\omega_c t))}{(1+t^2\omega_c^2)^{\frac{s}{2}}} - 1 \right), \quad (23)$$

where the relations $2\alpha(0) = \eta\omega_c^2\Gamma(1+s)$, $\int_0^\infty \alpha(\tau)d\tau = -i\lambda/\hbar$ and $\eta = 2\lambda/(\hbar\omega_c\Gamma(s))$ were used. The second term, $Q_2(t)$, includes the influence of the coupling to the leads on the dynamics of the reaction mode. The long-time limit of the reaction mode is determined by the first term in Eq. (20), i.e.

$$\lim_{t \rightarrow \infty} \langle Q(t) \rangle = \lim_{t \rightarrow \infty} Q_1(t) = -n_\infty \sqrt{\frac{2\lambda}{s\hbar\omega_c}} \quad (24)$$

In Fig. 6 we plot the dynamics of the reaction mode for the same parameters used to generate the data in left set of panels Fig. 4 for both the sub-Ohmic and super-Ohmic cases. Note that in both figures, we are unable to converge the results for $s = 2$ beyond the cutoff time $t_c = 100$ fs (see the discussion above). For $s \leq 1$, the reaction coordinate $\langle Q(t) \rangle$ decays monotonically to its steady state value if it is initially in equilibrium with the electronic state of the dot (full black and green lines). The timescale governing this decay can either be purely phononic, arising from the term $Q_1(t)$ with an algebraic relaxation characteristics given by $\sim (1+t^2\omega_c^2)^{-\frac{s}{2}}$, or associated with the relaxation of the electronic population $\delta n(t)$ arising from the term $Q_2(t)$. For $s = \frac{1}{2}$ the decay of $\langle Q(t) \rangle$ is significantly slower than that of $\delta n(t)$ and thus is determined by the slower phononic dynamics, while for $s = 1$ there is no clear time scale separation. In case of a preparation, where the phonon degrees of freedom are initially not in equilibrium with the electronic state of the dot (full red and blue lines), a more complex transient dynamics is seen, which involves electronic and phononic contributions and time scales.

In both cases ($s = \frac{1}{2}$ and 1), the dot population assumes for longer times two distinct values depending on the initial conditions for the phonon bath, i.e. exhibits bistability, as clearly evident in Fig. 4. The bistability in the dot populations leads to two solutions for $\langle Q(t) \rangle$. In the long-time limit, the difference between the solutions for $\langle Q(t) \rangle$, obtained for shifted and unshifted initial preparation, is related to the corresponding difference of the dot population Δn_d by^{65,82}

$$\Delta Q = -\frac{\lambda}{\hbar} \sqrt{\frac{2}{\alpha(0)}} \Delta n_d = -\sqrt{\frac{2\lambda}{s\hbar\omega_c}} \Delta n_d. \quad (25)$$

This relation between Δn_d and ΔQ is only valid in the steady state and can therefore be used as a consistency check if the steady state has been reached. For the results in Fig. 6 it is fulfilled.

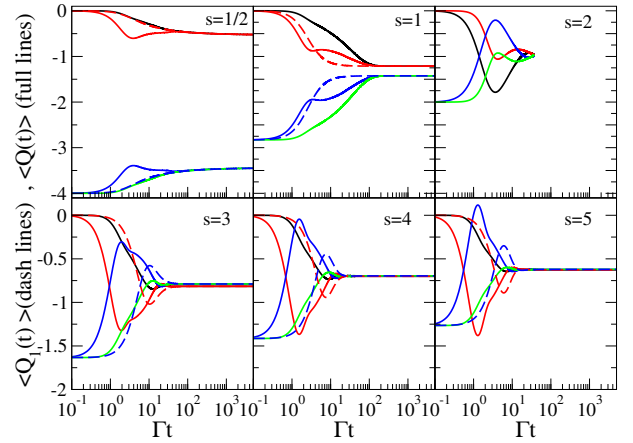


Figure 6: The reaction coordinate $\langle Q(t) \rangle$ for several values of s and for $\varepsilon_d = 0.25$ eV, $\lambda = 2000$ cm $^{-1}$ and $\omega_c = 500$ cm $^{-1}$ and temperature $T = 0$. Black - unoccupied $n_d(0) = 0$ and $\delta_j = 0$; Red - occupied $n_d(0) = 1$ and $\delta_j = 0$; Blue - unoccupied $n_d(0) = 0$ and $\delta_j = 1$; Green - occupied $n_d(0) = 1$ and $\delta_j = 1$. In addition, the dashed lines depict $Q_1(t)$, the part of $\langle Q(t) \rangle$ which describes the relaxation of the reaction mode due to the coupling to the phonon bath in the absence of coupling to the leads (see Eq. (21)).

As s is increased above 1 the picture changes qualitatively. First, the bistability gradually disappears as discussed in details above. This implies that $\langle Q(t \rightarrow \infty) \rangle$ assumes a unique value regardless of the initial preparation of the phonons. Second, as clearly evident in Fig. 6, $\langle Q(t) \rangle$ shows a pronounced oscillatory behavior correlated with the oscillations observed in the dot population shown in Fig. 4. Most interestingly, for the unshifted initial phonon preparation ($\delta_j = 0$), the oscillation in $\langle Q(t) \rangle$ lead to transient values for the reaction coordinate that are associated with the shifted position, and vice versa. This “exchange” of positions is also reflected, to a smaller extent, in the dot population shown in the corresponding panels of Fig. 4. For larger values of s ($s > 1$), the bare phonon relaxation time scale $\sim (1+t^2\omega_c^2)^{-\frac{s}{2}}$ is significantly faster than the electronic dynamics $\delta n(t)$, and thus the latter dominates the dynamics of the reaction mode $\langle Q(t) \rangle$ for longer times.

Conclusions

In this work we have studied the role of the spectral density of the phonon bath on the relaxation dynamics and bistability in the nonequilibrium extended Holstein model. To this end, sub-Ohmic, Ohmic and super-Ohmic spectral densities were considered. The results show a physically rich behavior, including a transition from incoherent to oscillatory dynamics and a disappearance of bistability signatures upon increase of the power s of the spectral density. Some features observed for the sub- and super-Ohmic cases can be rationalized qualitatively by rescaling the characteristic phonon frequency,

$\omega_c \rightarrow s\omega_c$. For example, the bistability which is exemplified in adiabatic limit $\omega_c \rightarrow 0$, persists over a larger range of frequencies for sub-Ohmic spectral density while the opposite is true for the super-Ohmic case. However, the appearance of a slow algebraic decay for $\langle Q(t) \rangle$ in the sub-Ohmic case as well as the oscillatory behavior of $\langle Q(t) \rangle$ in the super-Ohmic case cannot be explained by simple scaling arguments, but require a more elaborate analysis in terms of the bath correlation function, $\alpha(t)$ and are distinct from the Ohmic limit.

Acknowledgments

EYW is grateful to The Center for Nanoscience and Nanotechnology at Tel Aviv University for a doctoral fellowship. HW acknowledges the support from the National Science Foundation CHE-11500285. MT acknowledges support by the German Research Council (DFG) and the German-Israeli Foundation for Scientific Research and Development (GIF). This work used resources of the National Energy Research Scientific Computing Center, which is supported by the Office of Science of the U.S. Department of Energy under Contract No. DE-AC02-05CH11231, and the Leibniz Computing Center (LRZ) Munich. ER acknowledges support from the University of California start-up funds.

Appendix A: Reaction Coordinate Formal Solution

In this appendix we describe the formal solution of the reaction coordinate $Q(t)$ for both initial conditions (for simplicity we set $\hbar = 1$). For the phonon Hamiltonian

$$H_{ph} = \sum_j \omega_j \left(b_j^\dagger b_j + \frac{1}{2} \right) + d^\dagger d \sum_j M_j \left(b_j^\dagger + b_j \right), \quad (\text{A1})$$

the equation of motion for $b_j(t)$ reads

$$\dot{b}_j(t) = -i\omega_j b_j - iM_j d^\dagger d \quad (\text{A2})$$

with the formal solution

$$b_j(t) = b_j(0) e^{-i\omega_j t} - iM_j \int_0^t n_d(\tau) e^{-i\omega_j(t-\tau)} d\tau. \quad (\text{A3})$$

We will define the dimensionless average position of the phonon mode j with $\langle x_j(t) \rangle = \frac{\langle b_j^\dagger(t) + b_j(t) \rangle}{\sqrt{2}}$ and the corresponding reaction coordinate $\langle Q(t) \rangle = \frac{\sum_j M_j \langle x_j \rangle}{\sqrt{\sum_j M_j^2}}$ such that:

$$\langle Q(t) \rangle = \frac{\Re \left\{ \sum_j M_j \langle b_j(t) \rangle \right\}}{\sqrt{2 \sum_j M_j^2}}. \quad (\text{A4})$$

Using Eq. (A3) we find

$$\begin{aligned} \langle Q(t) \rangle &= \frac{\sqrt{2}}{\sqrt{\sum_j M_j^2}} \sum_j M_j \cos \omega_j t \langle b_j(0) \rangle \\ &\quad - \frac{\sqrt{2}}{\sqrt{\sum_j M_j^2}} \int_0^t \langle n_d(\tau) \rangle \sum_j M_j^2 \sin \omega_j(t-\tau) d\tau. \end{aligned} \quad (\text{A5})$$

The equation above can be re-written in terms of the bath autocorrelation function given in Eq. (18) using the relations:

$$\begin{aligned} \sum_j M_j^2 e^{-i\omega_j t} &= \frac{1}{\pi} \int_0^\infty \pi \sum_\alpha M_j^2 \delta(\omega - \omega_j) e^{-i\omega t} d\omega \\ &= \frac{1}{\pi} \int_0^\infty J(\omega) e^{-i\omega t} d\omega \\ &= \alpha(t) \end{aligned}$$

and

$$\sum_j \frac{M_j^2}{\omega_j} e^{-i\omega_j t} = -i \int_0^t d\tau \alpha(\tau) + \lambda, \quad (\text{A6})$$

to reduce the formal solution of $\langle Q(t) \rangle$ into

$$\begin{aligned} Q(t) &= \sqrt{\frac{2}{\alpha(0)}} \Im \int_0^t \delta n(\tau) \alpha(t-\tau) d\tau \\ &\quad + \sqrt{\frac{2}{\alpha(0)}} n_\infty \Im \int_0^t \alpha(\tau) d\tau \end{aligned} \quad (\text{A7})$$

The equation above corresponds to the non-shifted bath initial condition *i.e.* $\langle b_j(0) \rangle = 0$, while for the shifted-bath ($\langle b_j(0) \rangle = -\frac{M_j}{\omega_j}$), the solution reads:

$$\begin{aligned} \langle Q(t) \rangle &= -\sqrt{\frac{2}{\alpha(0)}} \lambda + \sqrt{\frac{2}{\alpha(0)}} \Re \left\{ i \int_0^t d\tau \alpha(\tau) \right\} \\ &\quad + \sqrt{\frac{2}{\alpha(0)}} \Im \int_0^t \delta n(\tau) \alpha(t-\tau) d\tau \\ &\quad + \sqrt{\frac{2}{\alpha(0)}} n_\infty \Im \int_0^t \alpha(\tau) d\tau. \end{aligned} \quad (\text{A8})$$

In the above $\delta n(t) = \langle n_d(t) \rangle - n_\infty$ with $n_\infty = \lim_{t \rightarrow \infty} \langle n_d(t) \rangle$ and $\Re \{ \dots \}$ ($\Im \{ \dots \}$) are the real and imaginary parts respectively.

One can look at the steady state limit using the fact that $\lim_{t \rightarrow \infty} \sqrt{\frac{2}{\alpha(0)}} \Im \int_0^t \delta n(\tau) \alpha(t-\tau) d\tau \rightarrow 0$ since $\delta n(\tau)$ and $\alpha(\tau)$ approach zero for $\tau \rightarrow \infty$ and

$$\int_0^\infty \alpha(\tau) d\tau = -i\lambda \quad (\text{A9})$$

to obtain

$$\Delta Q = -\sqrt{\frac{2}{s\lambda\omega_c}}\lambda\Delta n \quad (\text{A10})$$

$$= -\sqrt{\frac{2\lambda}{s\omega_c}}\Delta n \quad (\text{A11})$$

where ΔQ and Δn_d are the steady state difference between the shifted and the non-shifted phonon bath for the reaction coordinate and the dot population respectively.

-
- ¹ R. Hanson, L. Kouwenhoven, J. Petta, S. Tarucha, and L. Vandersypen, *Rev. Mod. Phys.* **79**, 1217 (2007).
 - ² C. Tannoudji, C. Dupont-Roc, and G. Grynberg, *Atom Photon Interaction: Basic Processes and Application* (New York: Wiley, 1992).
 - ³ R. A. Marcus, *Rev. Mod. Phys.* **65**, 599 (1993).
 - ⁴ U. Weiss, *Quantum Dissipative Systems* (World Scientific, Singapore, 1999).
 - ⁵ Y. Makhlin, G. Schön, and A. Shnirman, *Rev. Mod. Phys.* **73**, 357 (2001).
 - ⁶ A. J. Leggett, S. Chakravarty, A. Dorsey, M. P. Fisher, A. Garg, and W. Zwerger, *Rev. Mod. Phys.* **59**, 1 (1987).
 - ⁷ F. B. Anders, R. Bulla, and M. Vojta, *Phys. Rev. Lett.* **98**, 210402 (2007).
 - ⁸ A. Alvermann and H. Fehske, *Phys. Rev. Lett.* **102**, 150601 (2009).
 - ⁹ S. Chakravarty, *Phys. Rev. Lett.* **49**, 681 (1982).
 - ¹⁰ A. Bray and M. Moore, *Phys. Rev. Lett.* **49**, 1545 (1982).
 - ¹¹ R. Bulla, N.-H. Tong, and M. Vojta, *Phys. Rev. Lett.* **91**, 170601 (2003).
 - ¹² L. Serrano-Andres, M. Merchan, and A. C. Borin, *Proc. Natl. Acad. Sci. U.S.A.* **103**, 8691 (2006).
 - ¹³ A. Bray and N. Moore, *Phys. Rev. Lett.* **49**, 1545 (1982).
 - ¹⁴ S. Chakravarty, *Phys. Rev. Lett.* **49**, 681 (1982).
 - ¹⁵ S. Kehrein, A. Mielke, and P. Neu, *Z. Phys. B* **99**, 269 (1996).
 - ¹⁶ H. Spohn, *Comm. Math. Phys.* **123**, 277 (1989).
 - ¹⁷ M. Keil and H. Schoeller, *Phys. Rev. B* **63**, 180302 (2001).
 - ¹⁸ F. Anders and A. Schiller, *Phys. Rev. B* **74**, 245113 (2006).
 - ¹⁹ R. Bulla, T. A. Costi, and T. Pruschke, *Rev. Mod. Phys.* **80**, 395 (2008).
 - ²⁰ M. Thoss, H. Wang, and W. H. Miller, *J. Chem. Phys.* **115**, 2991 (2001).
 - ²¹ H. Wang and M. Thoss, *New J. Phys.* **10**, 115005 (2008).
 - ²² H. Wang and M. Thoss, *Chemical Physics* **370**, 78 (2010).
 - ²³ R. Egger and C. H. Mak, *Phys. Rev. B* **50**, 15210 (1994).
 - ²⁴ N. Makri and D. E. Makarov, *J. Chem. Phys.* **102**, 4611 (1995).
 - ²⁵ L. Mühlbacher and R. Egger, *J. Chem. Phys.* **118**, 179 (2003).
 - ²⁶ D. Kast and J. Ankerhold, *Phys. Rev. Lett.* **110**, 010402 (2013).
 - ²⁷ M. Grifoni and P. Hänggi, *Phys. Rep.* **304**, 229 (1998).
 - ²⁸ J. Klein, A. Léger, M. Belin, D. Défourneau, and M. Sangster, *Phys. Rev. B* **7**, 2336 (1973).
 - ²⁹ C. Adkins and W. Phillips, *J. Phys. C: Solid State Phys.* **18**, 1313 (1985).
 - ³⁰ B. Persson and A. Baratoff, *Phys. Rev. Lett.* **59**, 339 (1987).
 - ³¹ M. Galperin, M. A. Ratner, and A. Nitzan, *J. Chem. Phys.* **121**, 11965 (2004).
 - ³² B. N. J. Persson and J. W. Gadzuk, *Surf. Sci.* **410**, L779 (1998).
 - ³³ M. Galperin, M. A. Ratner, and A. Nitzan, *Nano Lett.* **4**, 1605 (2004).
 - ³⁴ S. Kohler, J. Lehmann, and P. Hänggi, *Phys. Rep.* **406**, 379 (2005).
 - ³⁵ J. Repp, G. Meyer, S. Paavilainen, F. E. Olsson, and M. Persson, *Phys. Rev. Lett.* **95**, 225503 (2005).
 - ³⁶ R. Härtle, C. Benesch, and M. Thoss, *Phys. Rev. B* **77**, 205314 (2008).
 - ³⁷ J. Cuevas and E. Scheer, *Molecular Electronics: An Introduction to Theory and Experiment* (World Scientific, Singapore, 2010).
 - ³⁸ T. Holstein, *Ann. Phys. (Leipzig)* **8**, 325 (1959).
 - ³⁹ J. Koch and F. von Oppen, *Phys. Rev. Lett.* **94**, 206804 (2005).
 - ⁴⁰ M. Galperin, A. Nitzan, and M. A. Ratner, *Phys. Rev. B* **76**, 035301 (2007).
 - ⁴¹ J. S. Seldenthuis, H. S. van der Zant, M. A. Ratner, and J. M. Thijssen, *ACS nano* **2**, 1445 (2008).
 - ⁴² R. Härtle and M. Thoss, *Phys. Rev. B* **83**, 125419 (2011).
 - ⁴³ R. Hütten, S. Weiss, M. Thorwart, and R. Egger, *Phys. Rev. B* **85**, 121408(R) (2012).
 - ⁴⁴ X. Shi, X. Zheng, Z. Dai, Y. Wang, and Z. Zeng, *J. Phys. Chem. B* **109**, 3334 (2005).
 - ⁴⁵ C. Joachim and M. A. Ratner, *Proc. Nat. Acad. Sci. USA* **102**, 8801 (2005).
 - ⁴⁶ M. Galperin, M. Ratner, and A. Nitzan, *Nano Lett.* **5**, 125 (2005).
 - ⁴⁷ R. Pati, M. McClain, and A. Bandyopadhyay, *Phys. Rev. Lett.* **100**, 246801 (2008).
 - ⁴⁸ R. Härtle and M. Thoss, *Phys. Rev. B* **83**, 115414 (2011).
 - ⁴⁹ A. S. Alexandrov and A. M. Bratkovsky, *Phys. Rev. B* **67**, 235312 (2003).
 - ⁵⁰ M. Galperin, M. A. Ratner, and A. Nitzan, *Nano Lett.* **5**, 125 (2005).
 - ⁵¹ A. Mitra, I. Aleiner, and A. Millis, *Phys. Rev. Lett.* **94**, 076404 (2005).
 - ⁵² D. Mozyrsky, M. Hastings, and I. Martin, *Phys. Rev. B* **73**, 035104 (2006).
 - ⁵³ A. S. Alexandrov and A. M. Bratkovsky, *J. Phys. Condens. Matter* **19**, 255203 (2007).
 - ⁵⁴ M. Galperin, A. Nitzan, and M. A. Ratner, *J. of Phys.: Condens. Matter* **20**, 374107 (2008).
 - ⁵⁵ A. A. Dzhioev and D. S. Kosov, *J. Chem. Phys.* **135**, 174111 (2011).
 - ⁵⁶ K. F. Albrecht, H. Wang, L. Mühlbacher, M. Thoss, and A. Komnik, *Phys. Rev. B* **86**, 081412 (2012).
 - ⁵⁷ E. Y. Wilner, H. Wang, G. Cohen, M. Thoss, and E. Rabani, *Phys. Rev. B* **88**, 045137 (2013).
 - ⁵⁸ L. Mühlbacher and E. Rabani, *Phys. Rev. Lett.* **100**, 176403 (2008).
 - ⁵⁹ H. Wang and M. Thoss, *J. Chem. Phys.* **131**, 024114 (2009).
 - ⁶⁰ H. Wang, I. Pshenichnyuk, R. Härtle, and M. Thoss, *J.*

- Chem. Phys. **135**, 244506 (2011).
- ⁶¹ L. Simine and D. Segal, J. Chem. Phys. **138**, 214111 (2013).
- ⁶² G. Cohen and E. Rabani, Phys. Rev. B **84**, 075150 (2011).
- ⁶³ G. Cohen, E. Y. Wilner, and E. Rabani, New J. Phys. **15**, 073018 (2013).
- ⁶⁴ E. Y. Wilner, H. Wang, M. Thoss, and E. Rabani, Phys. Rev. B **89**, 205129 (2014).
- ⁶⁵ E. Y. Wilner, H. Wang, M. Thoss, and E. Rabani, Phys. Rev. B **90**, 115145 (2014).
- ⁶⁶ A. Caldeira and A. J. Leggett, Phys. Rev. Lett. **46**, 211 (1981).
- ⁶⁷ B. Kubala and F. Marquardt, Phys. Rev. B **81**, 115319 (2010).
- ⁶⁸ R. Leturcq, C. Stampfer, K. Inderbitzin, L. Durrer, C. Hierold, E. Mariani, M. Schultz, F. von Oppen, and K. Ensslin, Nat. Phys. **5**, 327 (2009).
- ⁶⁹ M. Cizek, M. Thoss, and W. Domcke, Phys. Rev. B **70**, 125406 (2004).
- ⁷⁰ A. Mitra, I. Aleiner, and A. Millis, Phys. Rev. B **69**, 245302 (2004).
- ⁷¹ J. Koch and F. von Oppen, Phys. Rev. Lett. **94**, 206804 (2005).
- ⁷² M. Galperin, M. A. Ratner, and A. Nitzan, J. Phys.: Condens. Matter **19**, 103201 (2007).
- ⁷³ C. Benesch, M. Cizek, J. Klimes, I. Kondov, M. Thoss, and W. Domcke, J. Phys. Chem. C **112**, 9880 (2008).
- ⁷⁴ S. Weiss, J. Eckel, M. Thorwart, and R. Egger, Phys. Rev. B **77**, 195316 (2008).
- ⁷⁵ P. Werner, T. Oka, and A. J. Millis, Phys. Rev. B **79**, 035320 (2009).
- ⁷⁶ J. Eckel, F. Heidrich-Meisner, S. G. Jakobs, M. Thorwart, M. Pletyukhov, and R. Egger, New J. Phys. **12**, 043042 (2010).
- ⁷⁷ P. Werner, T. Oka, M. Eckstein, and A. J. Millis, Phys. Rev. B **81**, 035108 (2010).
- ⁷⁸ D. Segal, A. J. Millis, and D. R. Reichman, Phys. Rev. B **82**, 205323 (2010).
- ⁷⁹ E. Gull, D. R. Reichman, and A. J. Millis, Phys. Rev. B **82**, 075109 (2010).
- ⁸⁰ G. Cohen, E. Gull, D. R. Reichman, A. J. Millis, and E. Rabani, Phys. Rev. B **87**, 195108 (2013).
- ⁸¹ M.-L. Zhang, B. J. Ka, and E. Geva, J. Chem. Phys. **125**, 044106 (2006).
- ⁸² It is noted that the corresponding relation in Ref. 65 misses a numerical factor of $\sqrt{2}$.